

*Dedicated to Professor Mircea Diudea
on the Occasion of His 65th Anniversary*

INFLUENCE OF THICKNESS ON THE PROPERTIES OF TiO₂ AND Ti(Nb)O₂ THIN FILMS

MIRELA SUCHEA^{a,b,c,*}, MARIA VAMVAKAKI^d,
DIMITRIS LOULOUidakis^a, MICHAEL SIGALAS^e,
NIKOLAOS KATSARAKIS^{a,b}, DIMITRA VERNARDOU^{a,b},
EMMANUEL KOUDOUMAS^{a,b}

ABSTRACT. Pure and Nb doped titanium dioxide films were grown by magnetron sputtering, for integration in hybrid polymer-semiconductor solar cells. The effect of the thickness of the films on their physical properties was investigated, emphasis given on the optical transparency, the surface morphology, the wettability and the conductivity. Particular surface parameters were determined and their variation with film thickness was investigated. Finally, a hydrophobic to hydrophilic transition under UV irradiation was studied.

Keywords: metal oxides, titanium dioxide, thin films, thickness, solar cells applications.

INTRODUCTION

Titanium dioxide (TiO₂) is a wide energy gap semiconductor, with its conduction band minima composing of the Ti 3d band and its valence maxima composed primarily of the O 2p states. As a result of oxygen deficiency and the occupied defect states, TiO_x (x < 2) is an n-type semiconductor, typically

^a Center of Materials Technology and Photonics, School of Engineering Technological Educational Institute of Crete, 71004 Heraklion, Greece

^b Electrical Engineering Department, School of Engineering Technological Educational Institute of Crete, 71004 Heraklion, Greece

^c "Al.I. Cuza" University of Iasi, 11 Bulevard Carol I, Iasi, 700506, Romania, Romania

^d Department of Materials Science and Technology, University of Crete, 70013 Heraklion, Greece

^e Department of Materials Science, University of Patras, 26504 Rio, Patras, Greece

* Corresponding Author: mirasucnea@staff.teicrete.gr

used as an electron transporting material in dye sensitized solar cells, [1, 2]. However, the traditional preparation methods of nano-crystalline TiO_2 are not compatible with processing of polymer solar cells. Moreover, high temperatures (450°C) required to obtain crystalline TiO_2 cannot be used for both polymers and plastic substrate processing, in the corresponding flexible version. Finally, mesoporous TiO_2 films obtained from the TiCl_4 precursor [3] have a large roughness and are not effective as an electrode interlayer. As a result, most TiO_2 films used for polymer solar cells are in amorphous phase, made as an example by a sol-gel process.

In such a case, the solution precursor is typically prepared using titanium isopropoxide, along with various solvent additives. After spin coating, TiO_2 films are formed upon hydrolysis at a temperature of about 150°C . Using such amorphous TiO_2 films, both conventional and inverted polymer solar cells have been fabricated and studied. In conventional cells, the incorporation of TiO_2 as an electron transporting layer resulted in enhanced short circuit currents and fill factors, when compared with those in devices using aluminum electrodes only. Using PCDTBT:PC71BM as the active medium, the optimum devices presented a power conversion efficiency of 6.1% [4], the enhancement of the power conversion efficiency attributed to the improved electrical coupling with PC71BM and the enhanced light harvesting due to optical interference with the TiO_2 film, acting as an optical spacer [5]. In bulk heterojunction solar cells, an active layer as thin as 60–80 nm is usually a good strategy, for polymers with low hole mobility and high absorption coefficient, since the optical field distribution in the absorber is sensitive to its distance from the back electrode, making the I–V characteristics highly dependent on the spacer thickness [6]. When TiO_2 was used as the bottom electrode interlayer, with PEDOT: PSS/gold as the top electrode, the power conversion efficiency of the resulting inverted P3HT:PC71BM cells was about 3% [7, 8]. TiO_2 has also been used as an n-type material for the interconnecting charge recombination layer for solution processed tandem polymer solar cells. With P3HT:ICBA and PDTS-BTD:PC71BM as the two absorbing layers, a power conversion efficiency of 7% [9] was reported.

Organic–inorganic photovoltaic cells based on conjugated polymers and inorganic semiconductors have attracted a great interest as an alternative type of polymer solar cells, as a trial in developing low-cost, large-area, flexible photovoltaic devices, due to the advantage of high electron mobility and excellent chemical and physical stabilities of the inorganic semiconductors [10–14]. In this type of device, an electron-donor material (p-type conjugated polymers, such as poly(3-hexylthiophene) (P3HT)) and an electron-acceptor material (n-type inorganic nanocrystals, such as CdSe, TiO_2 , ZnO and CdS) are used as the active layer, which can form polymer-nanoparticle bulk heterojunctions [15–23]. Broad visible-infrared absorption, higher charge carrier mobility, and suitable electronic energy levels of both the donor and the acceptor

materials are important parameters for high-efficiency polymer solar cells. To balance exciton dissociation and charge transport, an ideal configuration of polymer-inorganic photovoltaic cell should be a columnar segregated donor/acceptor structure, with the size of each donor or acceptor section within the exciton diffusion length, perpendicular to the device electrodes, to provide unconstrained way for charge carrier transport. Nanostructured TiO₂ thin films and nanostructures with large surface-to-volume ratio in highly ordered arrays or less ordered structures could be involved to facilitate separation of the photo-excited charges and provide excellent electron percolation pathways for fabricating high performance organic-inorganic photovoltaic cells.

TiO₂ films are promising photoanode structures for the polymer-inorganic photovoltaic cells if provided: (a) an effective method for their transfer onto conductive transparent layers, that can ensure perfect electrical contact; (b) a spectral response broader than their limited UV absorption (<387 nm); (c) appropriate wettability of their surface, that could be tuned, so that high-quality polymer-TiO₂ interfaces can be obtained, since TiO₂ is hydrophilic, while polymers are hydrophobic. The present study is focused on the effect of thickness on the physical properties of pure and Nb doped TiO₂ thin films, grown by magnetron sputtering.

RESULTS AND DISCUSSION

TiO₂ and Ti(Nb)O₂ thin films with thickness in the range 50 to 1000nm were grown onto Corning 1737F glass substrates, in an 100% argon atmosphere and deposition parameters: total pressure (8×10^{-3} mbar), substrate temperature 27°C (RT) and plasma current $I=0.45$ A. The films were characterised and their properties were analysed, so that these can be optimized for energy applications.

XRD characterization of all deposited films showed that these were amorphous, a result in agreement with previous studies on TiO₂ based thin films, deposited at room temperature (RT) [24,25]. Electrical measurements performed before and after UV irradiation, using the two-point method on films with ohmic contacts, showed that pure, as well as the Nb doped TiO₂ films were insulators. The films were found to be highly transparent in the visible wavelength region, with an average transmittance of 70-80% in both pure and doped case, the respective transmission being slightly higher for Nb doped films, as shown in Figure 1a. It is interesting to note that the transmittance in the visible does not seem to be strongly affected by the thickness, at least for the range of thicknesses studied. This can be seen in the Figure 1b for TiO₂ films with thickness from 50 to 1000nm. AFM images of the surfaces of the TiO₂ and

Ti(Nb)O₂ thin films with different thickness are shown in Figure 2. The images revealed a clear tendency for an increasing of the lateral grain size with increasing the thickness, from 12 to about 40 nm for TiO₂ films and 10 to 30 nm for Ti(Nb)O₂ films respectively. Larger thickness leads to the appearance of grain agglomerations on the film surface, with dimensions in the range of 100-200 nm. An example is shown in figure (2d) for the 1μm thick TiO₂ thin film, where RMS is about 10.53 nm, while z range is 63.19nm. In contrast, RMS of thinner films was quite smaller, being in the range of about 0.20 nm to 0.75 nm, the maximum height of the respective features on the surface being about 5 nm.

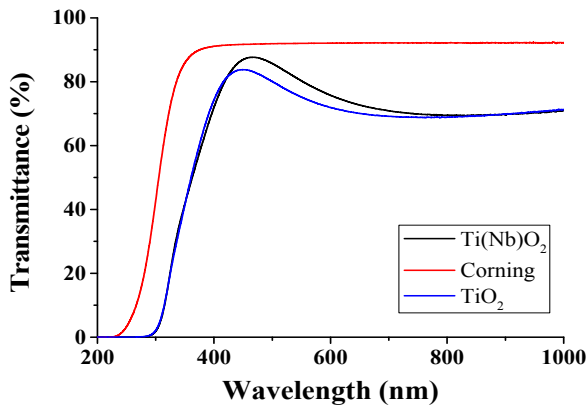


Figure 1a. UV-VIS transmission spectra of 100 nm TiO₂ and Ti(Nb)O₂ thin films

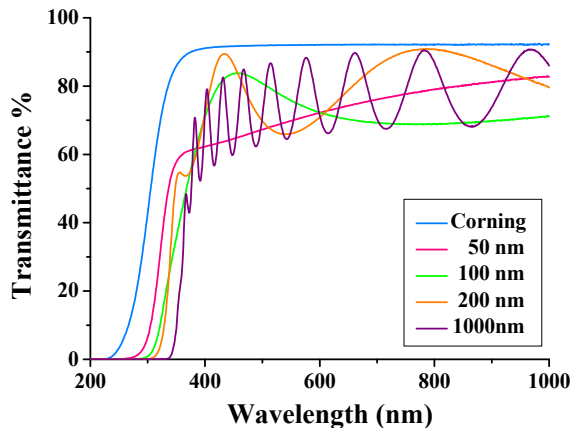


Figure 1b. UV-VIS transmission spectra of TiO₂ thin films with different thickness.

INFLUENCE OF THICKNESS ON THE PROPERTIES OF TiO₂ AND Ti(Nb)O₂ THIN FILMS

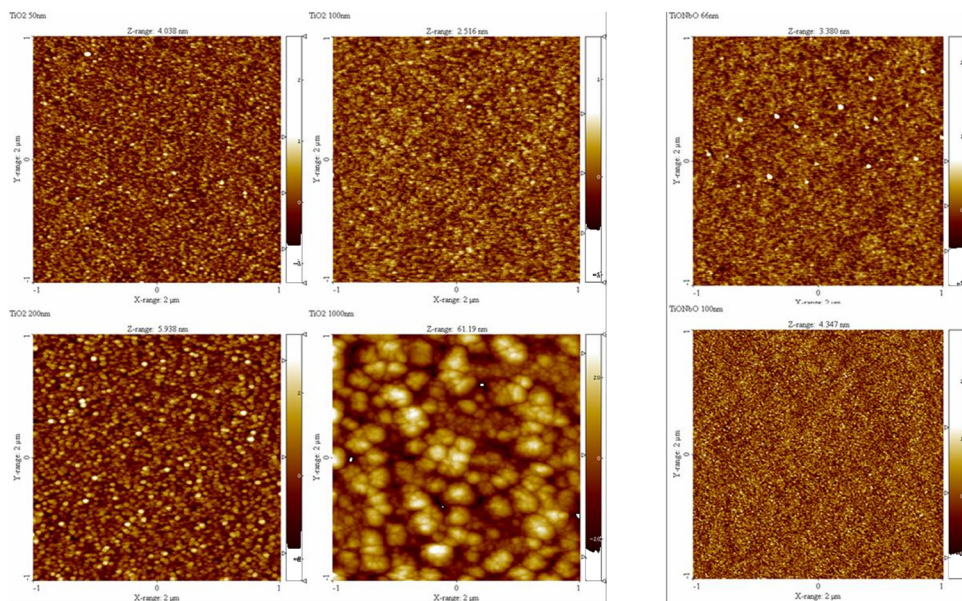


Figure 2. AFM images of TiO₂ films with different thickness (a: 50nm, b: 100nm, c: 200nm and d: 1 μ m) and (Nb)O₂ films (e: 66nm, f: 100nm). Scan size 2x2 μ m.

For more accurate description of the surface morphology, surface bearing index (S_{bi}), surface fractal dimension (SFD), skewness (SSK) and real surface ratio (SR) were also estimated. With increasing thickness, S_{bi} values were found to be almost constant, having values between 0.56 and 0.6 for pure TiO₂ and 0.6 to 0.64 for Nb doped films, while SR was increased from about 0.15% to over 6% in both cases. It is worth to mention that for similar thickness, Nb doped films showed overall larger SR and S_{bi} values. SFD and SSK were also found to increase with increasing thickness. Larger SFD values can be associated with higher compactness of the surface, while larger skewness reflects hill over valley domination. These variations are correlated with the film formation. In the case of thinner films, the growth time is shorter and the resulted surface exhibits a more homogeneous distribution of small grains, resulting in low RMS values. At the same time, SSK, SFD and SR values are small due to the large concentrations of valley like boundaries. For longer deposition periods, small grains aggregation leads to the formation of larger grains with a subsequent increase in the measured lateral grain size, leading to an overall “bulkier”, rougher film, with larger active surface. Nb doping of thin films seems to induce a slight decrease of the lateral surface grains size, resulting lower roughness, but also improved homogeneity and higher SSK, SFD and SR values with respect to those of the pure TiO₂ films.

The TiO₂ thin films were found to exhibit an amphiphilic behavior, since the surface was formed by both hydrophilic and hydrophobic domains. Those domains are generated mainly by the molecules adsorbed on the surface, this phenomenon occurring because the crystalline lattice tends to extend, in order to achieve similar vicinity for the surface atoms as for those of the bulk material and because the surface atoms are bond deficient. Due to this property, reversible transitions from hydrophobic to hydrophilic surface behavior can be achieved. Surface amphiphilicity is determined by the growth conditions.

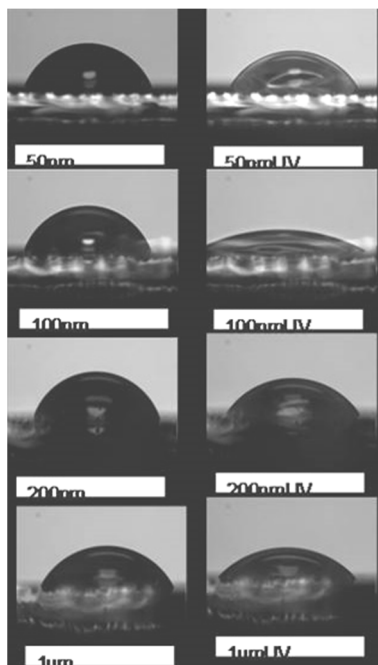


Figure 3a. Photos of water droplets on the surface of the TiO₂ films

The sessile drop geometry was then employed to determine the contact angle of water on the TiO₂ film surfaces. The method is based on the principle that the profile of a sessile drop of one fluid is governed by a balance between the surface/interfacial tensions. The advantage of this method for the determination of the contact angles is the fact that one uses the whole drop profile and not just the contact points with the substrate surface, since then, the actual value of the contact angle is extracted from the data and is not affected by possible impurities at the drop edges at the surface. Each drop (10 μL) of distilled, deionised Millipore water (18.2 MΩ) was formed from a capillary tip, and was detached gently upon the substrate of interest. The atmosphere around the droplet was kept rich in water vapours, in order to achieve minimum evaporation. The contact angle was then calculated by integration of the best-fit differential

equations that characterize the droplet shape. Moreover, in order to check the contact angle after the photo-reduction of the surface, the samples were directly irradiated in air by the UV light of a mercury pencil lamp at a distance of approximately 5 cm for 10 min, so that a steady state can be obtained. As found out, the contact angle depends on the film thickness, the respective dependence shown in Figure 3, which presents both photos of the water droplets on the surface of the films and the variation of the calculated contact angles with thickness before and after the UV irradiation. As can be seen, the contact angles are reduced after the UV irradiation, indicating a hydrophobic to

hydrophilic transition. Moreover, this transition was found to be more effective in the pure TiO₂ films and the films with larger thickness. Due to the fact that all experiments were performed in similar conditions, we can assume that the observed differences are due to the film surface. Then, we tried to correlate the observed changes with surface parameters calculated from AFM surface scans for the films. Figure 4 shows the variation of the contact angle after UV exposure with S_{bi} . As can be seen, increasing of S_{bi} results in a more hydrophilic behaviour.

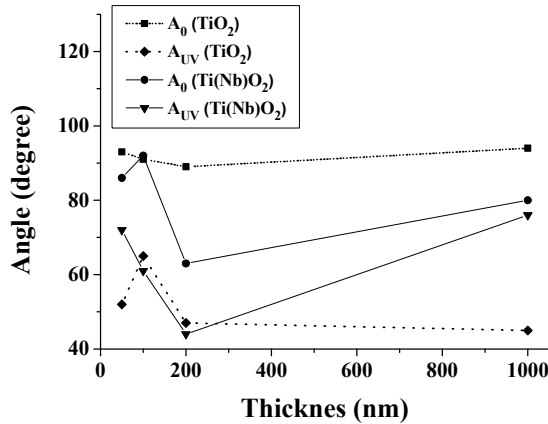


Figure 3b. Variation on contact angle as a function of thickness before (A_0) and after (A_{UV}) UV irradiation.

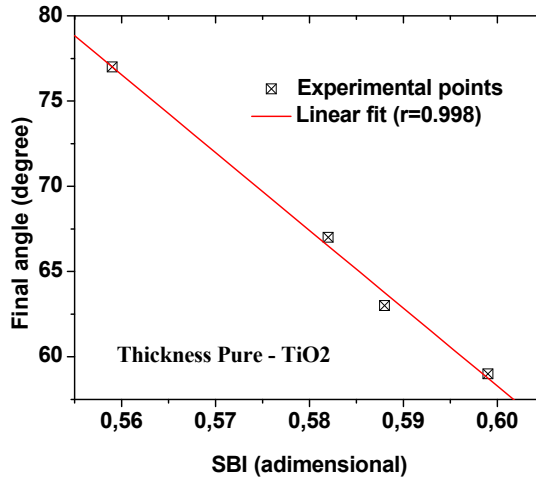


Figure 4. Contact angle variation with the S_{bi} after UV exposure.

S_{bi} is related to the material available for initial load support and it is defined as the ratio of the RMS deviation over the surface height at 5% bearing area.

$$S_{bi} = \frac{RMS}{Z_{0.05}} = \frac{1}{h_{0.05}}$$

where $h_{0.05}$ is the normalized surface height at 5% bearing area. A larger surface bearing index indicates a good bearing property. For a Gaussian height distribution, S_{bi} approaches 0.608 for increasing number of pixels.

The contact angle for water droplets deposited on clean films is linearly varying with the surface bearing index. The clean surface is obtained by irradiating the thin film with UV light.

Finally, the SR effect on the contact angle values before and after UV exposure is shown in figure 5. As can be seen, very small and very large values of SR result in small contact angles.

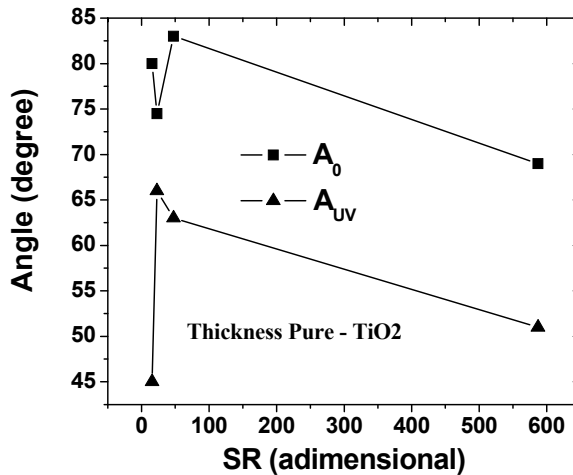


Figure 5. SR effect on the contact angle before and after UV exposure.

CONCLUSIONS

Pure and Nb doped titanium dioxide films were grown by magnetron sputtering for integration in hybrid polymer-semiconductor solar cells and the effect of film thickness on the physical properties of the films was investigated. As found out, under the used experimental conditions, the films are amorphous, highly transparent and of low conductivity. Moreover, thinner films exhibit a more homogeneous distribution of small grains, while, small grains aggregation

leads to “bulkier”, rougher films with larger active surface. Nb doping was found to induce a slight decrease of the lateral surface grains size, resulting lower roughness, but also improved homogeneity. Finally, the films surface was found to present a reversible transition from hydrophobic to hydrophilic, the overall behavior correlating the surface parameters.

EXPERIMENTAL SECTION

The deposition of the TiO₂ and Ti(Nb)O₂ films was carried out in an magnetron sputtering system using pure ceramic targets, total pressure 8×10^{-3} mbar, substrate temperature 27 °C (RT) and plasma current 0.45A. The thickness was measured using an in-situ thickness monitor and verified using a profilometer. AFM measurements were performed in air at RT using a Digital Instrument AFM with Nanoscope III controller in tapping mode. Ultra-sharp silicon cantilevers (NSC15 series, 125 mm long, spring constant ~ 40 N/m, resonant frequency ~ 200 -400 kHz) were used. The images were collected at 512×512 pixels per image at a scan rate of 1 Hz. In the present study the RMS (which is considered to be an index for the roughness), S_{bi} (surface bearing index) and SR (the ratio between real of the film surface and geometric scan surface) grain radius and features dimensions were evaluated using the Scanning Probe Image Processor, SPIP image processing software on the captured images. In order to study the crystal structure of the deposited films, X-ray diffraction (XRD) measurements were performed using a Discovery 8 diffractometer with CuK α X-rays. The optical transmittance was measured using a Shimadzu ultraviolet visible spectrophotometer (UV-Vis). Contact angle measurements were performed on as-deposited and during/ after 10 min UV exposure. Electrical measurements were performed using the two points method on films with Ohmic contacts, before and after UV exposure.

ACKNOWLEDGMENTS

This project is implemented through the Operational Program "Education and Lifelong Learning" action Archimedes III and is co-financed by the European Union (European Social Fund) and Greek national funds (National Strategic Reference Framework 2007 - 2013).

REFERENCES

1. B. Oregan and M. Gratzel, *Nature*, **1991**, 353, 737.
2. U. Bach, D. Lupo, P. Comte, J.E. Moser, F. Weissortel, J. Salbeck, H. Spreitzer and M. Gratzel, *Nature*, **1998**, 395, 583.

3. B.C. O'Regan, J.R. Durrant, P.M. Sommeling and N.J. Bakker, *J. Phys. Chem. C*, **2007**, *111*, 14001.
4. S.H. Park, A. Roy, S. Beaupre, S. Cho, N. Coates, J.S. Moon, D. Moses, M. Leclerc, K. Lee and A.J. Heeger, *Nat. Photonics*, **2009**, *3*, 297.
5. J.Y. Kim, S.H. Kim, H.H. Lee, K. Lee, W.L. Ma, X. Gong and A.J. Heeger, *Adv. Mater.*, **2006**, *18*, 572.
6. A. Roy, S.H. Park, S. Cowan, M.H. Tong, S.N. Cho, K. Lee and A.J. Heeger, *Appl. Phys. Lett.*, **2009**, *95*, 013302.
7. C. Waldauf, M. Morana, P. Denk, P. Schilinsky, K. Coakley, S.A. Choulis and C.J. Brabec, *Appl. Phys. Lett.*, **2006**, *89*, 233517.
8. T. Kuwabara, T. Nakayama, K. Uozumi, T. Yamaguchi and K. Takahashi, *Sol. Energy Mater. Sol. Cells*, **2008**, *92*, 1476.
9. J. Yang, R. Zhu, Z.R. Hong, Y.J. He, A. Kumar, Y.F. Li and Y. Yang, *Adv. Mater.*, **2011**, *23*, 3465.
10. L. Shen, G.H. Zhu, W.B. Guo, C. Tao, X.D. Zhang, C.X. Liu, W.Y. Chen, S.P. Ruan, *Appl. Phys. Lett.*, **2008**, *93*, 073307.
11. S. Tepavcevic, S.B. Darling, N.M. Dimitrijevic, T. Rajh, S.J. Sibener, *Small*, **2009**, *5*, 1776.
12. K.J. Jiang, K. Manseki, Y.H. Yu, N. Masaki, K. Suzuki, Y.L. Song, S. Yanagida, *Adv. Funct. Mater.*, **2009**, *19*, 2481.
13. Muktha, D. Mahanta, S. Patil, G. Madras, *J. Solid State Chem.*, **2007**, *180*, 2986.
14. M. Mall, P. Kumar, S. Chand, L. Kumar, *Chem. Phys. Lett.*, **2010**, *495*, 236.
15. R. Po, M. Maggini, N. Camaioni, *J. Phys. Chem. C.*, **2010**, *114*, 695.
16. N. Lu, S. Chen, H.T. Wang, X. Quan, H.M. Zhao, *J. Solid State Chem.*, **2008**, *181*, 2852.
17. K. Palaniappan, J.W. Murphy, N. Khanam, J. Horvath, H. Alshareef, M. Quevedo-Lopez, M.C. Biewer, S.Y. Park, M.J. Kim, B.E. Gnade, M.C. Stefan, *Macromolecules*, **2009**, *42*, 3845.
18. X.X. Jiang, F. Chen, H. Xu, L.G. Yang, W.M. Qiu, M.M. Shi, M. Wang, *Sol. Energy Mater. Sol. Cells*, **2014**, *94*, 338.
19. J.A. Labastide, M. Baghgar, I. Dujovnet, Y. Yang, A.D. Dinsmore, B.G. Sumpter, D. Venkataraman, M.D. Barnes, *J. Phys. Chem. Lett.*, **2011**, *2*, 3085.
20. M. Krunks, A. Katerski, T. Dedova, I.O. Acik, A. Mere, *Sol. Energy Mater. Sol. Cells*, **2008**, *92*, 1016.
21. J.S. Kim, Y. Park, D.Y. Lee, J.H. Lee, J.H. Park, J.K. Kim, K. Cho, *Adv. Funct. Mater.*, **2015**, *20*, 18.
22. Y.Y. Lin, T.H. Chu, C.W. Chen, W.F. Su, *Appl. Phys. Lett.*, **2008**, *92*, 0533121.
23. G.K. Mor, S. Kim, M. Paulose, O.K. Karghese, K. Shankar, J. Bsaham, C.A. Grimes, *Nano Lett.*, **2009**, *9*, 4250.
24. E.V. Buta, P. Pascariu, F. Prihor, L. Vlad, V. Pohoatã, R. Apetrei, D. Luca, A. Nastuță, I. Alupoaei, D. Mardare, *Scientific Annals of "Alexandru Ioan Cuza din Iași" University*, **2008**, Tomul I, 4.
25. D. Wicaksana, A. Kobayashi, A. Kinbara, *J. Vac. Sci. Technol. A*, **1992**, *10*, 1479.